Exploit the Performance of the Localization Algorithm for Wireless Sensor Networks under Gamma Radiation

Y. Liu[1], K. Colins[1] and L. Li[2]

[1] Fuel and Fuel Channel Safety Branch, Canadian Nuclear Laboratories, Chalk River, Ontario, Canada, K0J 1J0

[2] Applied Physics, Canadian Nuclear Laboratories, Chalk River, Ontario, Canada, K0J 1J0

yu.liu@cnl.ca, karen.colins@cnl.ca, liqian.li@cnl.ca

Abstract

With the advancement of computer and communication technologies, Wireless Sensor Networks (WSNs) are increasingly used in nuclear and space applications to monitor radiation fields. The sensor data from the WSN is accompanied by the sensor node's location relative to a geographical map of the monitored region. For reasons of cost, power, and GPS inaccessibility, localization algorithms that do not rely on GPS technology are used in nuclear and space applications working in high intensity radiation environments since gamma-ray damage to semiconductor devices is cumulative and can result in the premature failure of WSN nodes. In this paper, the performance of localization algorithms is evaluated for WSNs in a gamma-ray radiation environment, using Network Simulator 2 (NS2) simulation and a statistical model based on experimental results of radiation-damage tests in the Gamma-220 facility at the Canadian Nuclear Laboratories (CNL). The resulting performance analyses provide useful design insights and considerations for nuclear and space applications.

Keywords: Gamma Radiation, Wireless Sensor Network, Localization Algorithm, Nuclear, Space

1. Introduction

Wireless Sensor Networks (WSNs) are increasingly used in many aspects of our daily life, research and industries, such as radiation dose monitoring systems, health-care systems and structural integrity monitoring. Such networks normally consist of a large number of tiny sensor nodes that self-organize themselves into an inter-communicating wireless network that collects ambient information. A sensor node is battery-powered, which consequently has a limited lifetime. A survey by Akyildiz et al. reported significant research into extending the lifetime of sensor nodes by application of intelligent-designed, energy-conserving algorithms at different layers of the protocol stack [1]. In contrast, the effects of gamma radiation on the lifetimes of WSN nodes have received scant attention.

In the fields of nuclear and space sciences, much work has been done in the past decade [2][3][4][5] for deploying WSN based radiation-monitoring systems. Although nuclear and space monitoring are important WSN applications, both of them may be involved in high dose rate radiation environments. For example, WSNs were deployed in the area of the Fukushima

Daiichi nuclear plant accident to monitor radiation levels [6]. Extended-lifespan space structures, such as the International Space Station (ISS), are susceptible to micro-meteoroid and orbital debris damage, and NASA utilizes WSNs to detect leaks due to these kinds of damage [5]. A common concern in nuclear and space applications is the high radiation environment. These applications are referred to as “radiation-sensitive applications”. High doses of gamma-ray radiation cause cumulative damage to WSN nodes, resulting in premature failure. Gamma-rays’ damaging mechanisms are described as, and specifically linked to, electronic parameter changes in detectors, transistors and integrated circuits [7].

The sensor data from a WSN is accompanied by the locations of individual nodes relative to a geographical map of the monitored region. For reasons of cost, power, and GPS inaccessibility, non-GPS localization algorithms are used in the nuclear and space applications working in a high intensity radiation environment. The premature failure of WSN nodes due to gamma-ray damage challenges the performance of non-GPS localization algorithms, as the non-GPS localization methods are sensitive to the network topology change. To the best of our knowledge, the performance impact has not until now been the subject of systematic investigation. Note that the premature failure of any individual GPS based WSN node has no impact to other nodes in the network so that the challenge is mitigated compared to the non-GPS based system.

Wireless Sensor Network localization algorithms may be divided into two categories, referred to as range-based and range-free. Typical range-based algorithms are characterized by Time Of Arrival (TOA), Time Difference Of Arrival (TDOA) location method, Received Signal Strength Indicator (RSSI), etc. [8]. Usually, range-based algorithms incur additional costs for extra hardware. On the other hand, the range-free approach locates non-anchor nodes by calculating their distances from a set of designated, but sparse, anchor nodes with known positions, also known as landmarks [8]. Nuclear and space applications almost invariably employ high-density networks with large numbers of nodes over large-scale areas, to provide high-resolution data. To reduce cost, range-free methods are most commonly used.

In this paper, performance parameters of three range-free localization algorithms are evaluated for WSNs in a simulated gamma-ray radiation environment. The particular subjects of investigation are the Centroid [9], Distance Vector-Hop (DV-Hop) [10], and Amorphous [12] algorithms. The failure probability density of individual WSN nodes caused by ionizing radiation damage is based on the results of irradiation tests performed in the Gamma-220 facility (Co-60 source) at the Canadian Nuclear Laboratories (CNL). To conduct the evaluations, the authors extended the NS2 [13] to support the simulation of radiation-dose dependent early failure of WSN nodes, and the concomitant effects on localization. The results of the performance analyses of the three range-free localization algorithms provide useful design insights and considerations for nuclear and space applications.

2. Radiation Damage Tests

2.1 Background

The term gamma-ray refers to electromagnetic radiation of an extremely high frequency, consisting of high energy photons. Gamma-rays are usually generated in isotopic decay, in which an atomic nucleus transitions from a high energy unstable state to a lower energy stable state. In outer space, cosmic radiation includes a large portion of gamma-rays from a number of sources (e.g., supernovae and the sun). In nuclear power plants, gamma-rays present a radiation safety hazard, the intensity of which is carefully monitored.

It is commonly known that gamma-rays are biologically hazardous. What is not as well known is that gamma-rays will also damage electronics. Semiconductor electronics are affected by two basic radiation damage mechanisms: displacement damage and ionization damage. Few systems are immune to either phenomenon and most are sensitive to both [7]. Ionization damage is mainly caused by gamma radiation in this context, which is the focus of this paper. Note that neutron and other ionizing radiation sources also damage electronics, which are subject for future study.

- **Displacement damage:** Incident radiation displaces silicon atoms from their lattice sites. The resulting defects alter the electronic characteristics of the crystal structure.

- **Ionization damage:** Energy absorbed by electronic ionization in insulating layers, predominantly SiO_2, liberates charge carriers, which diffuse or drift to other locations where they are trapped, leading to unintended concentrations of charge and, as a consequence, parasitic fields.

Radiation damage to electronics is a complicated phenomenon and plays a major role in the design of WSN applications intended for use in radiation environments. More information about the study of radiation effects in semiconductor electronics and the development of radiation-resistant integrated circuits can be found in the literature [7][14][15].

2.2 Gamma Radiation Test

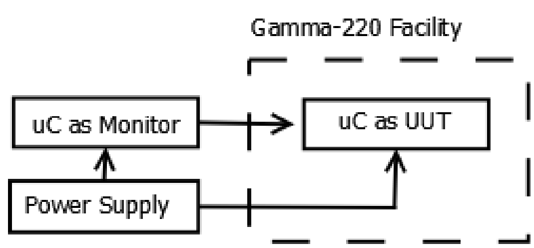

Figure 1 Block diagram of the radiation hardness test.

The WSN node used in this test consists of a micro-controller (µC) and some passive components. This test was to demonstrate that radiation hardness is determined primarily by µCs, and that passive components (e.g., resistors and capacitors) are relatively immune to radiation damage. The radiation hardness of the alternative µC will be used as the estimated radiation hardness of the WSN nodes [14]. Twenty four alternative µCs specifically programmed as Unit Under Test (UUT) were irradiated together in a Gamma-220 facility at CNL. The UUT continuously reported its self-check results to a universal monitor µC until the UUT was eventually damaged by the radiation. The framework of our radiation hardness test is shown in Figure 1, and the picture of our Gamma-220 facility and test board is shown in Figure 2.

Figure 2 The Gamma-220 facility at CNL. Left: Chamber open for setup; Middle: Chamber zoom-in; Right: Chamber lowered and test started.

The radiation dose response of individual µCs was characterized by a discrete numerical state variable on a domain representing 3 possible states. The variable → state relation was defined as (0 → normal), (1 → FLASH memory error), and (2 → unresponsive - dead). The state variables were measured at intervals of 4 seconds. The elapsed time of the constant-irradiation test was 24 hours at a dose rate of 0.196 kGy/h. The data showed that, contrary to initial expectations, the state transitions of individual µCs were reversible (see examples in Figure 3). That is, a dead µC could come back to life, at least temporarily. All possible state transitions (0→1, 0→2, 1→0, 1→2, 2→0, 2→1) were observed in the data. No state changes were recorded after 14 hours. Whether the observed state-change reversals were the result of an intrinsic recovery mechanism or radiation-stimulated reactivation is not known. This phenomenon might be partially related to the Single Event Upset (SEU) [16], but will be the subject of future study.

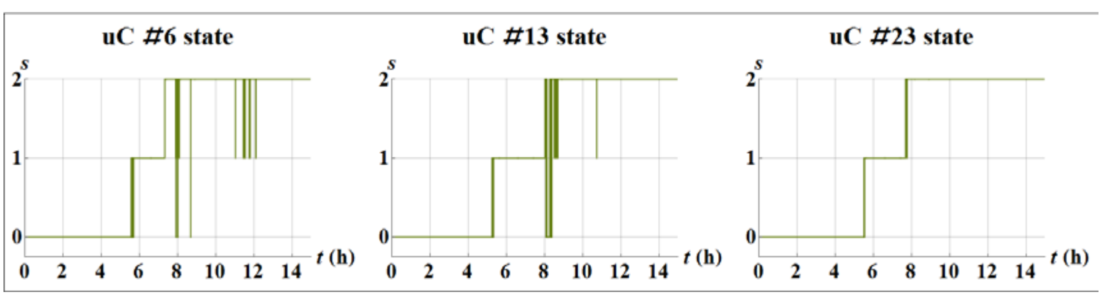

Figure 3 Example of µC state vs. time during gamma-ray irradiation.

The elapsed-time values of the entire set of state changes for all 24 µCs were transformed to absorbed-dose values. A histogram of the absorbed-dose values resembled the probability density function (PDF) of a Weibull distribution, as shown in Figure 4, with a shape parameter greater than unity, corresponding to a state-change rate that increased with dose.

The expression for the PDF of a random variate d obeying a Weibull distribution C is as shown in Equation 1 above, where α and β are shape and scale parameters, respectively, and e is the base of the natural logarithm, or Napier's constant.

$$\mathrm{PDF}(C,d)=\alpha\left(\frac{1}{\beta}\right)^{\alpha}d^{\alpha-1}e^{\left(\frac{1}{\beta}\right)^{\alpha}\left(-d^{\alpha}\right)} \tag{1}$$

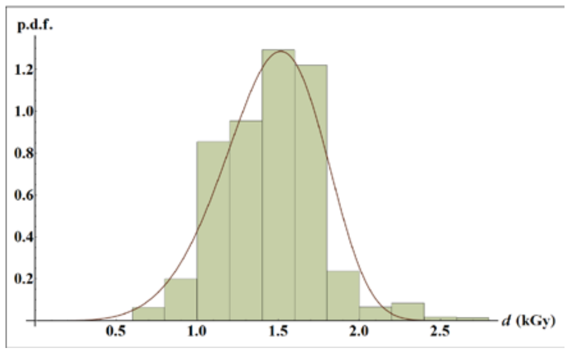

Figure 4 Absorbed-dose histogram and fitted PDF for Weibull-distributed μC state changes.

Taking the symbol d to represent the quantity absorbed-dose, a fitted PDF for Weibull-distributed μC state changes was obtained by finding values of the shape and scale parameters that yielded a match between the cumulants [17] of the expression for $\mathrm{PDF}(C,d)$ and those of the population of measured absorbed-dose values. The "*FindDistributionParameters*" function, within the computational software program Mathematica [17], was used to match the cumulants and compute the parameter values, $\alpha=5.4$ and $\beta=1.57$. The fitted PDF is plotted in Figure 4.

Section 4 of this paper describes a simulated WSN comprised of several hundred μCs characterized by radiation-dose dependent changes of state. The change of state of an individual μC was modelled as a random variate, given by a Weibull distribution with the fitted PDF shown in Figure 4.

3. Localization Algorithms

As mentioned in Section 1, range-free localization algorithms are more widely used in WSN, as it is a cost-effective alternative to more expensive range-based methods that require special hardware. The Centroid, DV-Hop, and Amorphous algorithm are typical range-free approaches, which are the focus of this paper.

In the Centroid algorithm, a heterogeneous network containing two types of WSN nodes, including the anchor nodes and regular nodes are used. Anchor nodes, which are a minority within the network, are with established location information, obtained from a GPS. Regular nodes, which are a majority within the network, are without GPS capacity so that they need to estimate their location through the Centroid method. Anchor nodes broadcast the beacons with their locations to their neighbours, the beacons flood through the network, and then all the nodes could receive them. The receiver node localizes itself to the region that coincides to the intersection of the connectivity regions of this set of reference points (a.k.a. Anchor Nodes, and their positions are denoted as (X_{i_k}, Y_{i_k})), which is defined by the centroid of these reference points (shown in Equation 2) [9].

$$\left(X_{est}, Y_{est}\right) = \left(\frac{X_{i_1} + \cdots + X_{i_k}}{k}, \frac{Y_{i_1} + \cdots + Y_{i_k}}{k}\right) \tag{2}$$

Similar to the Centroid algorithm, Anchor nodes in the DV-Hop method also flood the beacons with their locations through the WSN. However, the beacons not only bring the location information, but also a counter of the number of hops (a hop is one portion of the path between source and destination.). The receivers only keep the minimum counter value per anchor of all beacons to avoid the loopback hazard[1]. Then, all nodes obtain the shortest distance in hops to all the anchor nodes. Lastly, the hop count needs to be converted to physical distance by estimating the average distance per hop. The average hop-size is estimated by anchors i and j using the formula in Equation 3, where $(x_i, y_i), (x_j, y_j)$ are coordinates of anchors i and j, respectively, and h_{ij} is the number of hops between the two anchor nodes i and j [10].

$$HopSize_i = \frac{\sum_{j \neq i} \sqrt{(x_i - x_j)^2 + (y_i - y_j)^2}}{\sum_{j \neq i} h_{ij}} \tag{3}$$

Like the DV-Hop approach, the Amorphous method first obtains the shortest distance in hops to distributed anchors through beacon propagation to find the route with the minimum counter value. Then, this method uses the Kleinrock and Silvester formula, given in Equation 4, to estimate the average hop-size, which is different from the DV-Hop method. In this formula, n_{local} is the density of the network (defined as the number of nodes in the wireless signal transmission range) and Kleinrock and Silvester proved that $n_{local} = 6$ produces optimal network throughput for randomly distributed receivers [11]. The detailed information of this formula has been explained by Nagpal in [12]. Finally, triangulation is used to estimate the node's location as same as the DV-Hop algorithm.

$$HopSize = r\left(1 + e^{-n_{local}} - \int_{-1}^{1} e^{-\frac{n_{local}}{\pi}\left(\arccos t - t\sqrt{1-t^2}\right)} dt\right) \tag{4}$$

In addition, Triangulation (multilateration) is used for the DV-Hop and Amorphous methods to estimate the location of X when the estimated distance to at least three anchor nodes are obtained.

[1] Loopback refers to the routing of the beacons back to their source anchor nodes.

4. Evaluation Methodology

A simulated dynamic WSN was generated for the purpose of evaluating the performance of several localization algorithms, under the challenging condition of progressive radiation damage to the nodes of the network. The simulated WSN was comprised of several hundred µCs characterized by radiation-dose dependent changes of state. As mentioned previously in Section 2.2, the change of state of an individual µC was modelled as a random variate, given by a Weibull distribution with the fitted PDF shown in Figure 4.

The entire WSN was exposed to a simulated 2-dimensional gamma radiation field. The field was variable spatially but, for the sake of simplicity, assumed to be constant with respect to time. Thus, the radiation dose at each µC location increased linearly with elapsed time. At any point in time, the list of states of the entire population of µCs in the WSN was a key input parameter to the localization algorithms, which determined the concurrent communication connectivity graph that defines the interconnectivity of nodes of the WSN. Those µCs undergoing a state change of type normal → unresponsive (dead) became unavailable as a vertex in the connectivity-graph. The localization algorithms were therefore required to be executed at repeated intervals in time, in order to attempt to maintain effective and efficient communication throughout the WSN, as more µCs became unavailable with increasing time and dose. For simplicity, reversible state changes in µCs, evident from the plots in Figure 3, were not explicitly modelled — the simplifying assumption was made that all state changes were of the type normal → unresponsive (dead) and were irreversible.

For the localization algorithms evaluated, implemented on a simulated WSN through NS2, the authors evaluate the accuracy of the estimation by the Localization Error (LE), which represents the distance between the estimated location and the accurate location of WSN nodes. The LE is defined in Equation 5, where (x_{est}, y_{est}) is the estimated location and (x_a, y_a) is the actual location [9].

$$LE = \sqrt{(x_{est} - x_a)^2 + (y_{est} - y_a)^2} \tag{5}$$

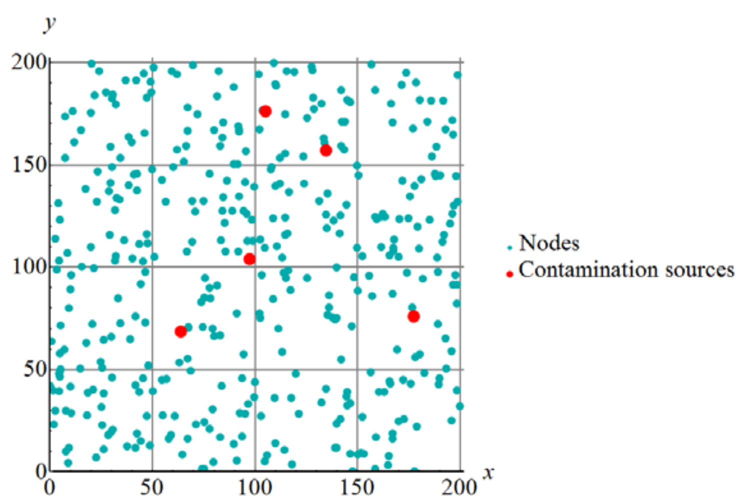

Figure 5 Node and source locations (arbitrary units).

In the simulated WSN, 400 nodes are deployed on a 2-dimensional square spatial domain, of side length 200 units. Of the 400 nodes, 12.5% or 50 are anchor nodes. The locations follow a uniform bivariate random distribution, as might occur if the sensors were all dropped from an airplane or drone flying in a regular pattern over the domain, resulting in a node density distribution that is relatively uniform everywhere. Simulated sources of radioactive contamination (e.g., the site of a nuclear reactor severe accident) and locations of all nodes in the network are shown in Figure 5. The source locations follow an asymmetric random bivariate distribution, as might occur in the layout of a multi-unit nuclear station.

In the simulation, the authors assumed that radioactive contamination was scattered by wind-affected deposition in the neighbourhoods of the source locations, with densities following distributions that follow normal distribution in the crosswind direction (parallel to the y axis) and follow skewed normal distribution in the downwind direction (parallel to the x axis and blowing from positive toward negative coordinates). It is further assumed that the quantities of radioactive contamination (i.e., radioactivity) originating from the 5 source locations are in relative proportion according to the randomly generated set of numbers (89, 35, 66, 76, 77). Figure 6 is a plot showing the spatial dependence of collective radioactive contamination originating from all 5 source locations, based on the previously stated assumptions. Units of these quantities are arbitrary, and are therefore not shown in the figure.

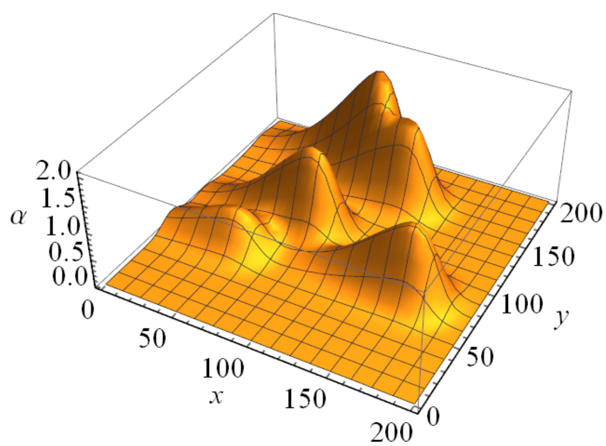

Figure 6 Activity density α (arbitrary units in all dimensions).

Using the inverse-square-law-dependence of dose rate on the distance of a contaminated surface-area-element from a node, the activity density can be integrated over all space to evaluate the total dose rate $\dot{d}_n$ at each of the 400 node locations (x_n, y_n), as shown in Figure 7. The integrated radiation dose rates corresponding to sensor node locations from Figure 5 are represented as a 3-dimensional triangular mesh in Figure 7, where the third coordinate of the vertex at $(x_n, y_n, \dot{d}_n)$ gives the simulated dose rate proximate to node n, located at the position given by the first and second vertex coordinates (x_n, y_n). Again, units of quantities are arbitrary, and therefore not shown in the figure.

When a node fails, a Tool Command Language (TCL) script [19] is generated corresponding to the node ID and time of failure through a Python script [20]. Through a data-file, all of the mesh data values $(x_n, y_n, \dot{d}_n)$ are explicitly read into the network simulation, so that the network simulation matches the radiation field and sensor-location distribution topologically. The transmission range is set as 50 m and IEEE 802.11 protocol stack [21] is used in the NS2 simulation.

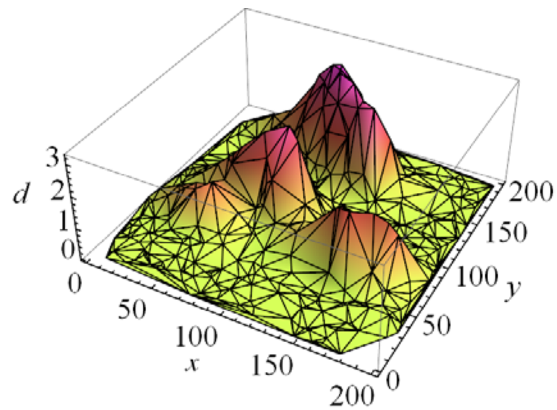

Figure 7 Radiation dose rate $\dot{d}$ (arbitrary units in all dimensions).

5. Results of Simulation

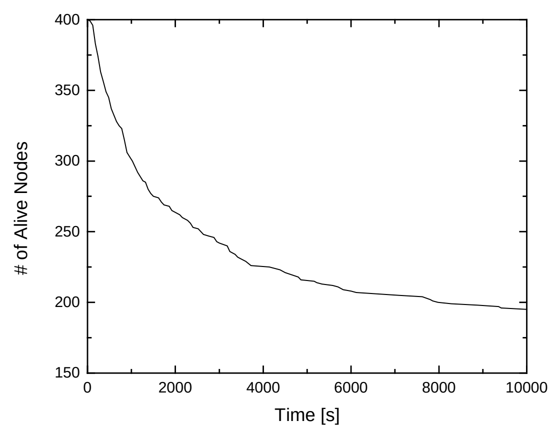

Figure 8 Number of alive nodes over time [s].

In this section, the simulation data and its analysis are presented. Figure 8 shows the number of active nodes during the elapsed time (1000 s) for all the experiments presented in this section. Nodes are provided with sufficient energy to ensure that they do not fail during the course of the simulation. As a result, all node failures are due to the simulated radiation damage, which is the focus of this paper. Note that both anchor nodes and regular nodes will fail due to the radiation damage in our simulation. The lifetime of all nodes depend on the radiation dose.

The authors compared the average LE per 100 s among Centroid, DV-Hop and Amorphous algorithms and 12.5% ratio of nodes are the anchor nodes in Figure 9. Interestingly, Centroid algorithm performs the best among them, although it is the simplest one. The reason is that the Centroid algorithm does not depend on the calculation of the average hop size. So, it is more resistant to the network topology change because of the premature failure of WSN nodes. Although DV-Hop method will calculate the hop size in the run-time, it is not sensitive to all kinds of topology changes. For example, the number of hops between anchor nodes is not significantly changed, whereas the hops between regular nodes and anchor nodes are significantly changed. The DV-Hop method cannot track this case. The Amorphous approach experiences a similar situation as the DV-Hop method, but its hop size estimation is off-line and the hop size will not be re-calculated during run-time. Consequently, the Amorphous approach demonstrates even worse performance than DV-Hop.

Note that the Centroid method even fairs better at the beginning of the simulation (the LE calculation starts time of 100 s). The locations of nodes follow a uniform bivariate random distribution to simulate the scenario that the sensors were all dropped from an airplane or drone flying in a regular pattern over the domain. In Figure 5, it can be observed that the actual distance between nodes is hard to be accurately calculated through the average hop size. That's the reason why the Centroid method performs best at the beginning. In addition, the failures of nodes start at the time of 180 s due to the high dose radiation sources.

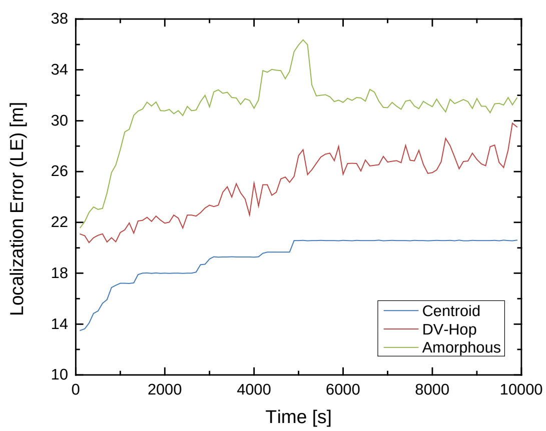

Figure 9 The Comparison among Centroid, DV-Hop and Amorphous algorithms.

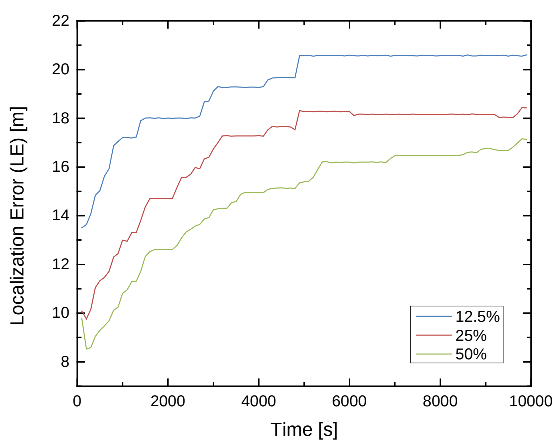

Figure 10 The average Localization Error (LE) over time of Centroid algorithm on different ratios of anchor nodes in the WSN.

In addition, the performance change of the average LE on different ratios of anchor nodes was evaluated through the Centroid algorithm in Figure 10, including 12.5%, 25% and 50% of anchor nodes in the network. In Figure 10, it is clear that the average LE drops with the increased anchor nodes in the WSN. The reason is that more anchor nodes are more resistant to the loss of reference points in the network. Note that the average LE enters a stable stage at around 5000 s. After the nodes close to the radiation sources were permanently damaged, the rate of losing the nodes greatly reduces, as the remaining nodes are far from the radiation sources. In addition, sometimes the loss of more nodes results in a slight performance improvement because the communication conflict reduces in certain areas. However, the trend of increasing average LE cannot be altered.

6. Conclusion

In this paper, the authors evaluated three WSN range-free localization algorithms in a large-scale gamma-ray radiation environment. The probability density function of a Weibull distribution was used to model state changes (including failure) of individual nodes in simulated WSNs. The distribution parameters were based on results of radiation-damage tests performed on semiconductor devices in the Gamma-220 facility at CNL.

In the non-radiation environment, it is well known that the Amorphous and DV-Hop algorithm offer the smaller localization error than the Centroid algorithm [10][12]. The simulation results in this paper disclose different results in the radiation environment that the Centroid method is best among the evaluated localization algorithms, which provide useful design insights and considerations for nuclear and space applications.

The reason is that the Centroid algorithm does not depend on the calculation of the average hop size. Therefore, it is more resistant to network topology changes resulting from node failures. The DV-Hop method is not sensitive to topology changes, if the number of hops between anchor nodes is not significantly changed although the hops between regular nodes and anchor nodes are dramatically changed. The Amorphous approach is in the similar situation as DV-Hop method, but its hop size estimation is calculated off-line and the hop size will not be re-calculated during run-time. Consequently, the Amorphous approach demonstrates even worse performance than DV-Hop.

The radiation oriented localization algorithm with adaptive hop size estimation, extended radiation damage tests to cover more devices (e.g. flash memory and RF chips), and neutron damage experiment to electronics are subject for the future study. In addition, different number of radiation sources and their distributions will be evaluated for better understanding the performance of localization algorithms under radiation environment.

7. References

[1] AKYILDIZ I.F., SU W., SANKARASUBRAMANIAM Y. and CAYIRCI E., Wireless Sensor Networks: a Survey, in the International Journal of Computer and Telecommunications Networking, Volume 38 Issue 4, pp. 393-422, 2002

[2] HUANG F. and SUN T., Design and Implementation of Radiation Dose Monitoring System Based on Wireless Sensor Network, in the Proceedings of the International Conference on Future Information Technology, Singapore, 2011

[3] FUJIWARA T. and TAKAHASHI H., Study on a Sensor Network System with a Self-Maintenance Function for Plant Monitoring System, in the Proceedings of Joint International Workshop: Nuclear Technology and Society – Needs for Next Generation, Berkeley, CA, 2008

[4] GOLDSMITH D., GAURA E., BRUSEY J. and SHUTTLEWORTH J., Wireless Sensor Networks for Space Applications—Thermal Monitoring for a Gas Turbine Engine, in the Proceedings of Nanotech Conference and Expo, Houston, TX, 2009

[5] WILSON W. and GARY A., Wireless Sensing Opportunities for Space Applications, in the Journal of Sensors and Transducers, 94(7), pp. 83-90, 2008

[6] BIELSA A., Detecting Radiation Levels in Fukushima: an example of crowdsourcing, http://www.libelium.com/fukushima_crowdsourcing_radiation_social_project, 2013 February

[7] SPIELER H., Introduction to Radiation-Resistant Semiconductor Devices and Circuits, in the Proceedings of 7th Workshop of Beam Instrumentation, Argonne, USA, 1996

[8] HE T., HUANG C., BLUM B., STANKOVIC J. and ABDELZAHER T., Range-free Localization Schemes for Large Scale Sensor Networks, in the Proceedings of ACM MobiCom, San Diego, CA, pp. 81-95, 2003

[9] BULUSU N., HEIDEMANN J. and ESTRIN D., GPS-less Low Cost Outdoor Localization for Very Small Devices, in the Journal of IEEE Personal Communications Magazine, 7 (5), pp. 28-34, 2000

[10] CHEN H., SEZAKI K., DENG P. and SO H.C., An Improved DV-Hop Localization Algorithm for Wireless Sensor Networks, in the Proceedings of the 3rd IEEE Conference on Industrial Electronics and Applications, 2008

[11] KLEINROCK L. and SILVESTER J., Optimum Transmission Radii for Packet Radio Networks or Why Six is a Magic Number, in the Proceedings of the National Telecommunications Conference, Birmingham, Ala., 1978 December 3-6

[12] NAGPAL R., Organizing a Global Coordinate System from Local Information on an Amorphous Computer, A.I. Memo 1666, MIT A.I. Laboratory, 1999 August

[13] NS2 website: http://www.isi.edu/nsnam/ns/

[14] LI L., WANG Q., BARI A., DENG C., CHEN D. and JIANG J., Field Test of Wireless Sensor Network in the Nuclear Environment, in the Journal of AECL Nuclear Review, Volume 3 No. 1, pp. 47-51, 2014

[15] MILLARD J., Radiation-tolerant electronics testing of a prototype isolating preamplifer, in the Journal of Fusion Engineering and Design, Volume 29, pp. 330–333, 1995

[16] WANG F. and AGRAWAL V., Single Event Upset: An Embedded Tutorial, in the Proceedings of 21st International Conference on VLSI Design, 2008

[17] ABRAMOWITZ M. and STEGUN I.A., (Eds.) Handbook of Mathematical Functions with Formulas, Graphs, and Mathematical Tables, 9th printing. New York: Dover, p. 928, 1972

[18] Mathematica document centre: http://reference.wolfram.com/language/

[19] TCL development website: https://www.tcl.tk/

[20] Python development website: https://www.python.org/

[21] IEEE 802.11 official website: http://www.ieee802.org/11/